Genome Biology

RESEARCH

Open Access

Molecular dependencies and genomic consequences of a global DNA damage tolerance defect

Daniel de Groot[1], Aldo Spanjaard[1], Ronak Shah[1], Maaike Kreft[1], Ben Morris[2], Cor Lieftink[2], Joyce J. I. Catsman[1], Shirley Ormel[1], Matilda Ayidah[1], Bas Pilzecker[1], Olimpia Alessandra Buoninfante[1], Paul C. M. van den Berk[1], Roderick L. Beijersbergen[2] and Heinz Jacobs[1*]

†Daniel de Groot and Aldo Spanjaard are joint first authors.

*Correspondence: h.jacobs@nki.nl

[1] Division of Tumor Biology & Immunology, The Netherlands Cancer Institute, Plesmanlaan 121, 1066 CX Amsterdam, The Netherlands
[2] Division of Molecular Carcinogenesis, The NKI Robotics and Screening Center, The Netherlands Cancer Institute, Plesmanlaan 121, 1066CX, Amsterdam, The Netherlands

Abstract

Background: DNA damage tolerance (DDT) enables replication to continue in the presence of fork stalling lesions. In mammalian cells, DDT is regulated by two independent pathways, controlled by the polymerase REV1 and ubiquitinated PCNA, respectively.

Results: To determine the molecular and genomic impact of a global DDT defect, we studied $Pcna^{K164R/-}$;$Rev1^{-/-}$ compound mutants in mouse cells. Double-mutant cells display increased replication stress, hypersensitivity to genotoxic agents, replication speed, and repriming. A whole-genome CRISPR-Cas9 screen revealed a strict reliance of double-mutant cells on the CST complex, where CST promotes fork stability. Whole-genome sequencing indicated that this double-mutant DDT defect favors the generation of large, replication-stress inducible deletions of 0.4–4.0 kbp, defined as type 3 deletions. Junction break sites of these deletions reveal microhomology preferences of 1–2 base pairs, differing from the smaller type 1 and type 2 deletions. These differential characteristics suggest the existence of molecularly distinct deletion pathways. Type 3 deletions are abundant in human tumors, can dominate the deletion landscape, and are associated with DNA damage response status and treatment modality.

Conclusions: Our data highlight the essential contribution of the DDT system to genome maintenance and type 3 deletions as mutational signature of replication stress. The unique characteristics of type 3 deletions implicate the existence of a novel deletion pathway in mice and humans that is counteracted by DDT.

Graphical Abstract

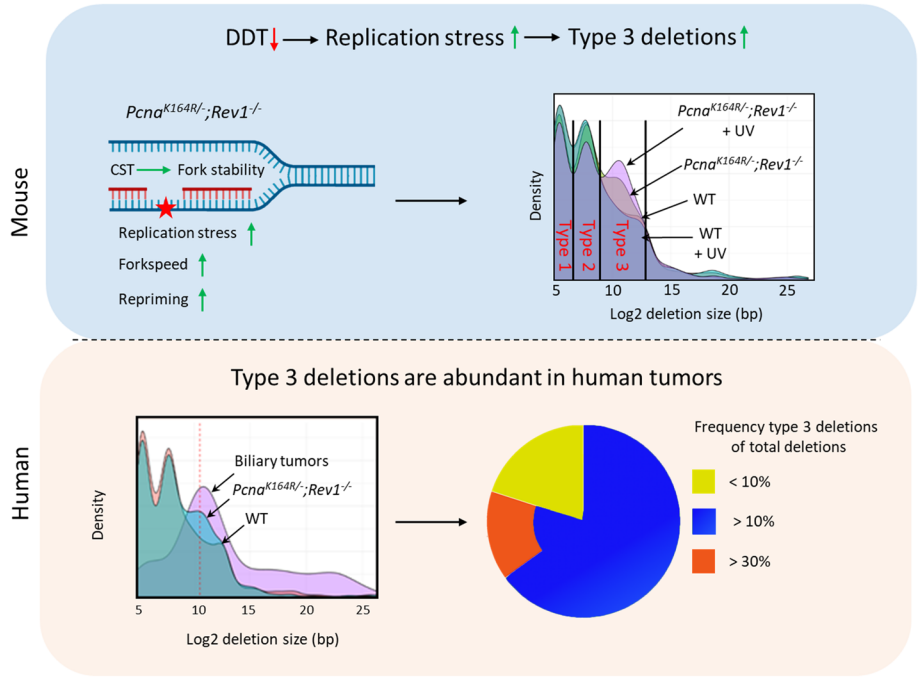

Background

Genomes are subjected to a continuous barrage of genetic insults. To preserve genetic information, genome maintenance is essential for life. A versatile DNA damage response (DDR) network warrants that most genotoxic lesions are sensed and restored effectively [1, 2]. Defects in DNA repair pathways can result in accelerated aging, increased tumorigenesis, sensitivity to DNA damage, and various developmental defects [1–8]. As DNA lesions usually arise in one of the two complementary strands, the repair synthesis of excision-based repair pathways strongly relies on the integrity of the complementary DNA strand. During replication, however, strand separation prohibits canonical excision repair of DNA lesions that persisted into S phase. These lesions can stall replicative DNA polymerases, which may result in a collapse of the replication fork and generation of more mutagenic secondary lesions such as DNA double strand breaks (DSBs) [9]. DSBs arising in S-phase are repaired in a relatively error-free manner by homology directed DSB repair (HR) which uses the intact template of the sister chromatid to bypass the lesion. However, alternative, more error-prone DSB repair pathways such as canonical non-homologous end joining (NHEJ) and alternative end joining (A-EJ) are active as well. These are associated with a broad spectrum of mutations, ranging from subtle InDels to structural variances such as deletions, chromosome rearrangements, and translocations [10, 11].

To bypass replication blocking lesions and simultaneously prevent recombinogenic DSBs, cells employ several DNA damage tolerance (DDT) pathways that enable replication to continue opposite DNA lesions, thereby stabilizing the replisome, thought to come at the expense of accuracy [10, 12–14]. In addition, DDT enables replicative

bypass of unhooked interstrand crosslink (ICL). In this way, DDT constitutes an integral, intermediate step in ICL repair pathways, including Fanconi anemia repair [4, 15, 16]. Furthermore, DDT can contribute to nucleotide excision repair (NER) [17]. Four distinct modes of DDT are distinguished: (i) translesion synthesis (TLS) opposite the lesion, (ii) template switching (TS), which takes advantage of the intact template of the sister chromatid avoiding the lesion, (iii) fork reversal (FR), during which the replication fork is remodeled into four-way junctions to avoid the lesion, and (iv) repriming behind the damaged template followed by gap filling TLS ("post-replicative" TLS) or by homology directed repair of the remaining gap ("post replicative" TS), though this mode of DDT is still poorly described and studied [18–21]. TLS utilizes specialized DNA damage tolerant Y-family DNA polymerases η (POLH), ι (POLI), κ (POLK), and REV1 and the B-family polymerase ζ (POLZ), which allows replication to continue directly opposite specific lesions [12, 22]. TLS polymerase recruitment is facilitated by damage-induced *mono*-ubiquitination of PCNA (PCNA-mUb) on lysine residue 164 [23, 24]. TS and FR depend on damage-induced *poly*-ubiquitination of PCNA (PCNA-Ub^{n}) at lysine residue 164 and avoid the lesion by continuing DNA synthesis on the newly synthesized intact template of the sister chromatid [25]. TLS polymerase REV1 has been implicated in the recruitment and activation of other Y-family TLS polymerases independent of PCNA-Ub through its C-terminal domain [26–29].

TLS is considered to be the predominant mode of DDT in mammals [30]. TLS polymerases—except REV—feature a capacious active site that can incorporate bulky nucleotides and non-Watson–Crick base pairs [31–33]. Moreover, in contrast to replicative polymerases, TLS polymerases are proof-read incompetent as they lack the 3′-5′ exonuclease domain to remove "misincorporated" bases. Consequently, as shown in gapped plasmid assays, replication opposite non-instructive lesions can be highly error prone [12, 34–36]. Based on these in vitro observations TLS, as predominant arm in mammalian DDT, is in general considered mutagenic. In contrast, TLS can also be error-free, as is the case for POLH, which can tolerate specific UV lesions [37]. Xeroderma pigmentosum variant (XP-V) patients that lack POLH activity have an increased risk of developing skin cancer upon UV exposure [5]. DDT is observed in all domains of life; it is an important building block of the mammalian DNA damage response network and essential for mammalian life [38, 39]. The sum of these insights suggests an important contribution of DDT to genomic integrity in the context of genotoxic lesions and fork-stalling structural impediments in the DNA template.

Our previous studies documented an essential, non-redundant contribution of PCNA-Ub and REV1 controlled DDT for mammalian development, stem cell maintenance, and drug responsiveness [38, 40]. We here defined the molecular and genomic impact of a compound DDT defect. To accomplish this goal, we generated lymphoma cell lines that were deficient for both PCNA-Ub and REV1. These mutations were found associated with increased sensitivity to most replication blocking agents, replication stress, and replication fork speed. The latter related to increased single-strand gaps, indicating increased repriming activity as a remaining alternative to bypass lesions to warrant fork stability. Furthermore, to define molecular dependencies and backup mechanisms of cells suffering from a global DDT defect, we performed an unbiased genome wide

CRISPR-Cas9 drop out screen. This screen identified the CST complex, comprising CDC13/CTC1, STN1, and TEN1, as essential for cell survival and cell cycle progression of DM cells. CST is involved in telomere capping and regulates telomerase and DNA polymerase alpha-primase (polα-primase) access to telomeres [41]. Apart from its telomere function, the CST complex mediates DNA end protection by blocking MRE11 mediated degradation of nascent DNA strands, thereby protecting stalled replication forks [41–43]. Recently, CST has also been found to directly control fork progression through modulation of DDR activity [44], https://doi.org/https://doi.org/10.1126/sciadv.add8023**,** to counteract toxicity of oxidative damage [45], and to be required for survival in yeast deficient for Rad6 [46]. Though a role of CST in repriming has been proposed [47], our DNA fiber assays rather support a function in fork stabilization. Surprisingly, further genomic characterization of $Pcna^{K164R/-}$;$Rev1^{-/-}$mutation revealed that the accumulation of small-scale mutations was not grossly altered, as shown by whole-genome sequencing (WGS). Instead, our analyses revealed a multimodal size distribution of genomic deletions, each of which was characterized by a preferential 1–3-bp micro-homology pattern at the break/junction sites. Notably, the DDT defect favored a specific accumulation of UV damage inducible, large type 3 deletions ranging between 0.4 and 4.0 kbp in size, likely as a consequence of replication stress. To extrapolate the impact and relevance of our findings to the human system, we took advantage of the WGS database of human tumors as provided by the Hartwig Medical Foundation (HMF). Remarkably, deletions of similar size were found abundant in human cancers. These deletions appear to increase in the presence of DDR defects and decrease upon amplification of defined DDR genes and appear affected by the treatment modality. The sum of our insights highlights the critical contribution of the DDT system in genome maintenance, both in human and mice. A multimodal size distribution of deletions and selective micro-homology preferences implicate distinct repair activities underlying their generation. We propose type 3 deletions as a replication stress associated and damage-inducible mutational feature, which suggests the existence of a specific deletion pathway that is counteracted by DDT.

Results

DDT-deficient cells lacking PCNA-Ub and REV1

Previous work in our lab established a non-epistatic and embryonic lethal interaction of a $Rev1^{-/-}$ and the $Pcna^{K164R/K164R}$ mutation (Additional file 1: Fig. S1A) [7, 38]. In contrast to single mutants, a compound mutant was found to be synthetic lethal in primary MEFs (Additional file 1: Fig. S1B). Ablation of p53 rescued this synthetic lethality (Additional file 1: Fig. S1B). Based on this knowledge, we made a thymic lymphoma cell line that was established from a $p53^{-/-}$;$Pcna^{K164R/loxP}$ mouse, as described previously [48]. Using this as a founder cell line, we established genetically defined isogenic $Pcna^{wt/-}$;$Rev1^{wt/wt}$ (WT) and double-mutant $Pcna^{K164R/-}$,$Rev1^{-/-}$ (DM) lymphoma cell lines. Two isogenic clones of both DM and WT were generated and used in all experiments to exclude interclonal variations. This provided a useful tumor model to study the relevance of DDT in DNA damage response and mutagenesis. As expected, a compound mutant DDT defect led to a profound increase in the sensitivity to various genotoxic

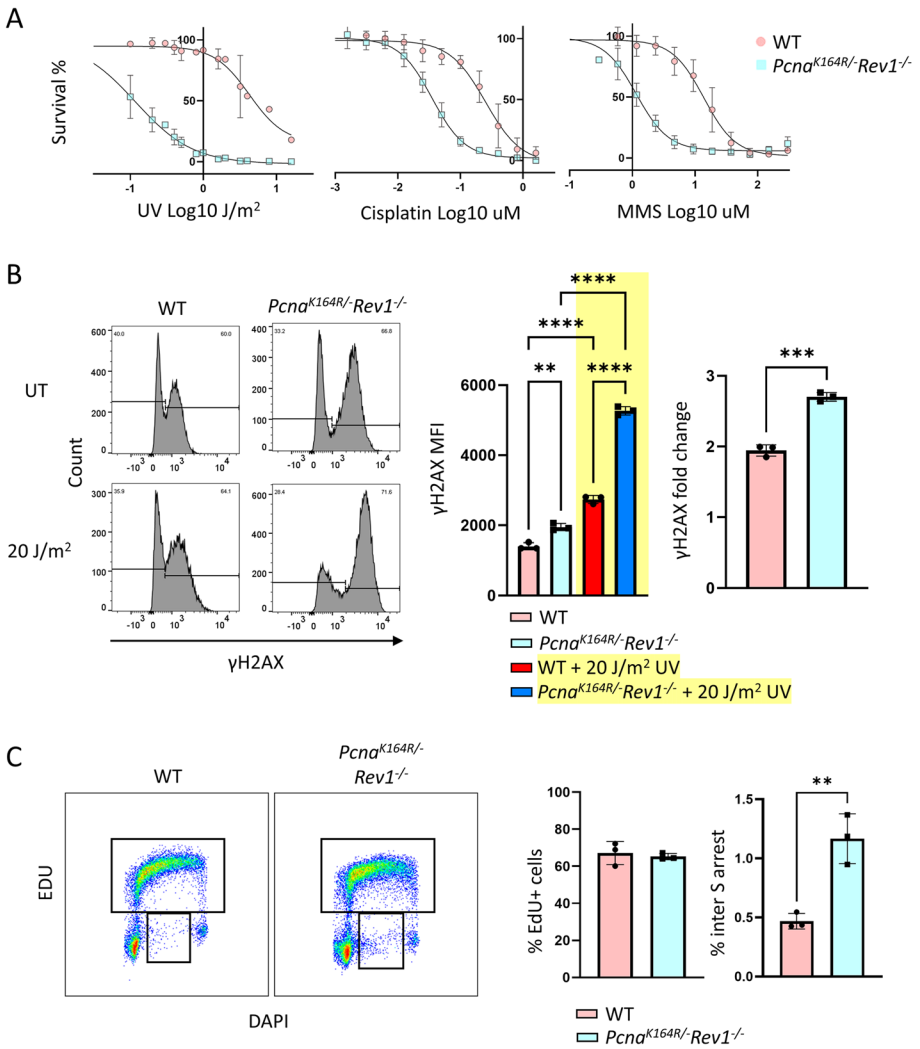

Fig. 1 Consequences of DDT deficiency upon genotoxic stress and the cell cycle. **A** Survival curves of WT and DM lymphomas upon exposure of UV-C, cisplatin, or MMS. **B** Replication stress by mean fluorescent intensity (MFI) of γH2AX with or without UV-C exposure in lymphomas. (left) Histograms are from a representative experiment, (right) bar graph of the γH2AX MFI from the γH2AX positive population as indicated in the histograms. **C** Analysis and quantification of cell cycle progression via EdU incorporation in unperturbed WT and DM lymphomas

agents (Fig. 1A). The DM cells were hypersensitive to UV-C induced lesions, cisplatin, and the alkylating agent methyl methanesulfonate (MMS). In line with these results, an unbiased high throughput compound screen revealed many more compounds to which specifically DM lymphomas were highly sensitive. These either directly damage DNA (e.g., carboplatin, RITA NSC65287, and melphalan) or alter DNA metabolism (e.g., 6-thioguanine) or act as cell cycle inhibitors (CB1954) (Additional file 1: Fig. S2A-D). Intriguingly, one of the only compounds DM cells appeared more resistant to then WT cells was 5-fluorouracil (Additional file 1: Fig. S2C and S2D), a finding consistent with a previous study [49].

To confirm that the hypersensitivity of the DM related to increased replication stress, we determined the levels of phosphorylated H2AX (γH2AX) as a marker for DNA

damage and replication stress. Mean fluoresce intensity (MFI) of γH2AX was used as a relative measure of replication stress. Without treatment, the levels of γH2AX in the DM were modestly increased compared to WT. In line with the hypersensitivity, treatment with a high dose of UV-C (20 J/m^2) further increased replication stress 4 h after exposure in both the DM and WT. Again, DM displayed much higher levels (Fig. 1B, Additional file 1: Fig. S3A), indicating that the sensitivity to endogenous and exogenous genotoxins directly relates to the level of replication stress as measured by the accumulation of γH2AX.

As replication stress was increased in untreated conditions, we set out to determine the effect of a compound DDT defect on the cell cycle as determined by incorporation of the thymidine analogue EdU (5-ethynyl-2′-deoxyuridine) in combination with the DNA stain DAPI. Somewhat surprisingly, a 20-min pulse of EdU followed by flow cytometry failed to reveal a significant difference in the frequency of cells in S phase in DM (Fig. 1C, Additional file 1: Fig. S3B). However, a significant increase of S phase cells that failed to incorporate EdU was found in the DM (Fig. 1C). These cells likely activated an intra S checkpoint prior to the EdU pulse, resulting in an intra S phase arrest. Apparently, under endogenous stress conditions the cell cycle of most DM cells was unaffected, implying a similar rate of division but slight increase of intra-S aborted cells.

Reliance of DDT deficient cells on CST

To investigate molecular dependencies and potential backup mechanisms of DDT in DM cells, we took advantage of WT and DM lymphoma cells to perform an unbiased whole-genome dropout screen in unperturbed conditions (Fig. 2A). Upon stable expression of Cas9 in DDT-proficient WT and DDT-deficient DM cells, we used the YUSA V2 library (Tzelepis et al., 2016 [50]), containing ≈ 79,000 guides that target most murine protein-coding genes. We observed an excellent R^2 of 0.7–0.8 between independent replicates in both WT and DM cell conditions and moreover observed decreases of guides targeting essential genes over time, whereas non-essential genes remained unaltered (Additional file 1: Fig. S4A). Importantly, DM cells did not feature proliferation defects, which allowed us to directly compare both isogenic cell lines without confounding issues resulting from differential stress signals and replication defects. Among other interesting potential hits, two of the three components of the CST complex, TEN1 and CTC1, were readily identified, with the third component, STN1 (encoded by *Obfc1*), being just below the significance cutoff (Fig. 2B).

(See figure on next page.)

Fig. 2 Investigation of the molecular dependency of DDT deficient cells. **A** Schematic overview of CRISPR-Cas9 whole-genome dropout screen. **B** Overview of the results from the CRISPR-Cas9 whole-genome dropout screen. **C** Western blot showing ablation of the STN1 protein in the lymphomas. (1)WT, (2) *Pcna*$^{K164R/-}$;*Rev1*$^{-/-}$, (3) *BCL2*^{OE};*Obcf1*$^{-/-}$;*Pcna*$^{K164R/-}$;*Rev1*$^{-/-}$, (4) *BCL2*^{OE};*Abcg8*$^{-/-}$;*Pcna*$^{K164R/-}$;*Rev1*$^{-/-}$. **D** Survival curves of STN1 KO and control lymphomas upon exposure of cisplatin or MMS. **E** Replication stress by MFI of γH2AX with or without UV-C exposure in STN1 KO and control lymphomas. (left) Histograms are from a representative experiment, (right) bar graph of the γH2AX MFI from the γH2AX positive population as indicated in the histograms. **F** Analysis and quantification of cell cycle progression via EdU incorporation in unperturbed STN1 KO and control lymphomas

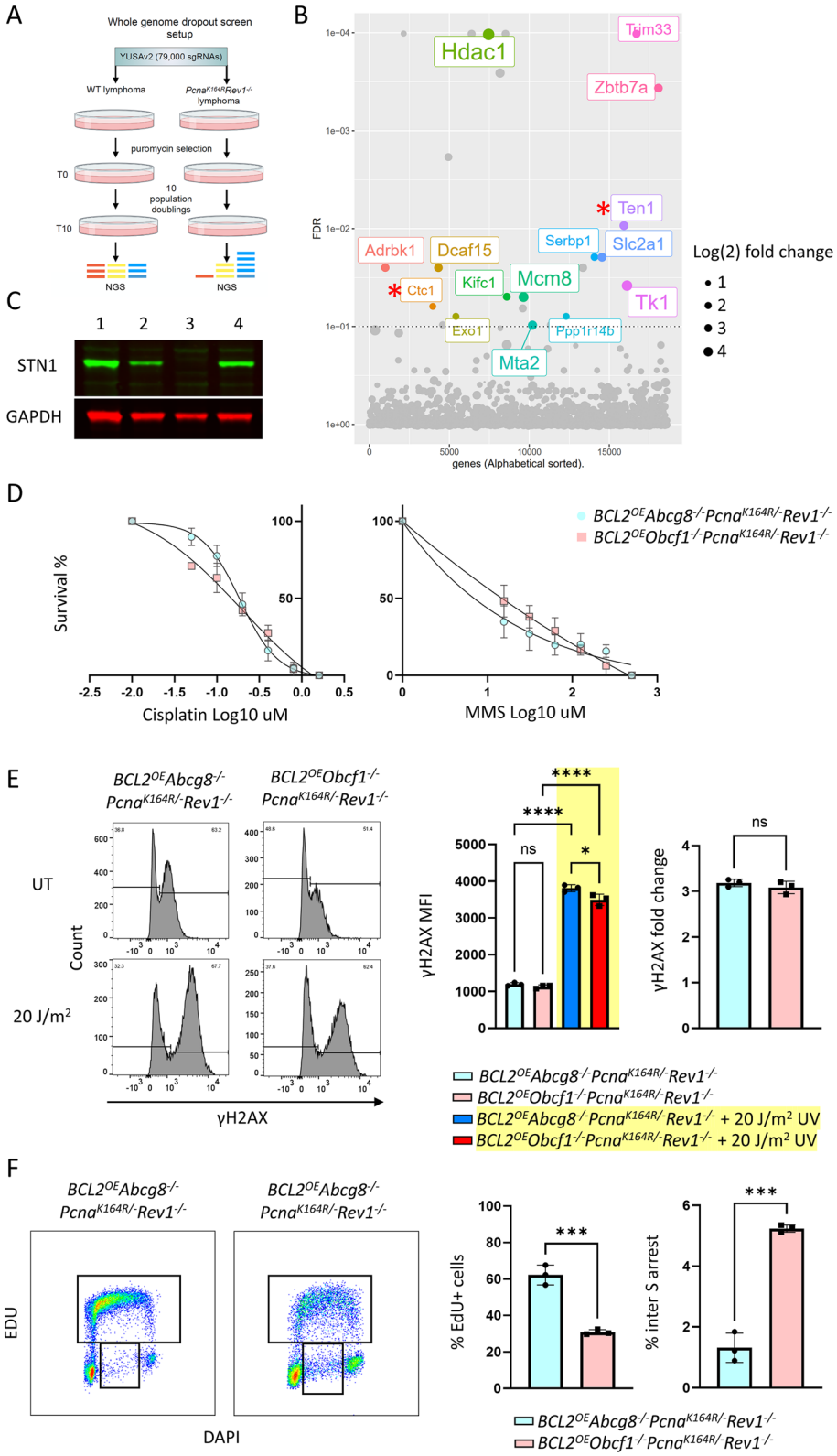

Fig. 2 (See legend on previous page.)

Interestingly, we did not find PrimPol, an important polymerase involved in repriming, suggesting that repriming capacity is not crucial for survival of DM cells.

To validate the dependence of DM cells on CST, we opted for a STN1 knockout in the DM lymphomas, as STN1-specific antibodies were available. In line with the screen, we failed to derive a viable cell line. However, upon overexpression of the anti-apoptotic factor BCL2 in the DM setting, we were able to establish a STN1 KO in these cells (Fig. 2C). The BCL2 overexpression system allowed further exploration of the molecular relevance of CST in the DDT deficient cells. As a transduction control, the *Abcg8* gene was used, a gene commonly used as control gene in whole-genome CRISPR screens. When exposed to cisplatin or MMS, CST-deficient DM cells did not show a marked increase in sensitivity compared to the BCL2 overexpressed control (Fig. 2D, Additional file 1: Fig. S4B and S4C). This suggests that CST is not directly involved in DDT of these specific exogenous lesions.

In support of this notion, the MFIs of γH2AX were found comparable between the BCL2 control and its STN1 KO (Fig. 2E). A slight decrease in replication stress was found upon UV treatment, though comparison of the fold changes seems to negate this difference. The level of replication stress correlated with drug sensitivities (Fig. 2D, 2E).

Strikingly, using EdU to investigate the cell cycle profile revealed drastic changes in the STN1 KO (Fig. 2F). The number of EdU positive cells was severely reduced; the number of EdU negative inter S phase arrested cells was found increased (Fig. 2F). This suggests a role of CST in stabilizing replication during endogenous stress.

Taken together, unlike DM cells, the changes in the cell cycle of the STN1 KO are not reflected by an increase in replication stress. In a DDT-deficient setting, the primary role of CST in prohibiting replication stress appears to relate to endogenous replication impediments rather than coping with specific exogenous lesions.

Efficient repriming increases fork speed in DDT deficient cells

As DDT is primarily demanded and activated during genome replication and DM displayed increased replication stress, we studied replication fork progression using the DNA fiber assays to visualize and analyze individual replicons (Fig. 3A) [51]. Under standard culture conditions, we observed a significant increase in the replication speed in DM lymphomas (Fig. 3B). This likely relates to repriming upon encountering a lesion,

(See figure on next page.)

Fig. 3 Replication fork speed and S1 nuclease assay in DDT deficient lymphomas and STN1 KO. **A** Schematic representation of the DNA fiber labeling experiment. The upper panel represents the two labeling periods and ongoing replication fork without encountering exogenous lesions. The lower panel illustrates the replication fork encountering a UV-C induced lesion. **B** (Left) Replication speed, lymphomas were first labeled with CldU for 20 min and then exposed to 20 J/m^2 UV-C or mock treatment, followed by 60 min labeling with IdU. The lengths of IdU tracks were measured and the average replication speed (kb/min, error bar indicates standard deviation) is displayed. (Right) IdU track length with or without S1 treatment and UV-C. Same labeling and treatment strategy was used as for replication speed assays. *P* values are based on Kruskal–Wallis test, *$P < 0.05$, **$P < 0.01$, ***$P < 0.001$, ****$P < 0.0001$. **C** Schematic representation of the DNA fiber labeling experiment with S1 nuclease digestion. In the upper panel a ssDNA gap is illustrated in the second label (IdU). After S1 nuclease treatment, in the lower panel, the ssDNA gap is cleaved, and a shorter IdU track length is left. **D** Same as in B but with the STN1 KO lymphoma and control

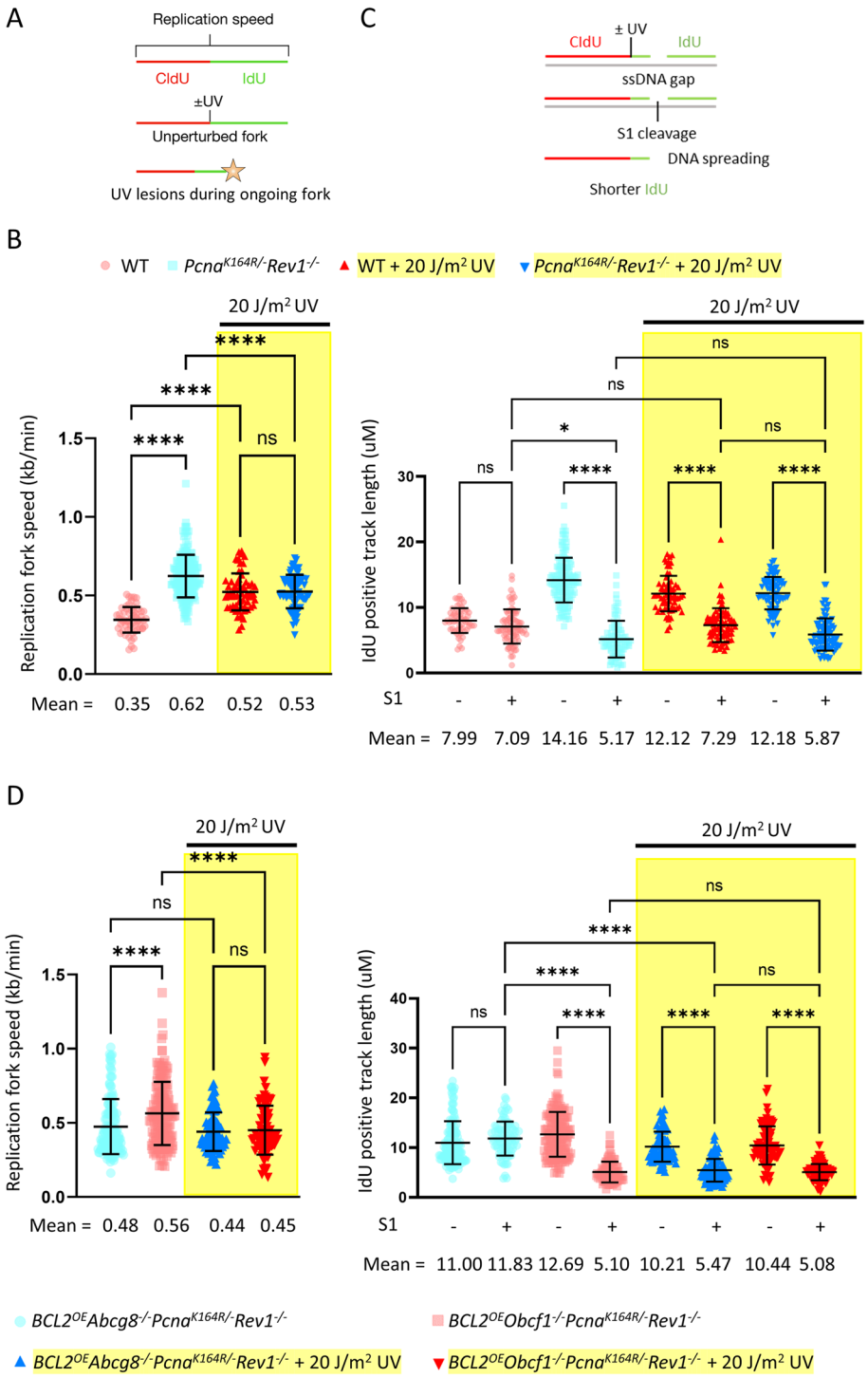

Fig. 3 (See legend on previous page.)

as one of the few options left to the DM cells. Upon UV-C exposure, a decrease in fork speed in the DM was observed, while an increase was found in WT cells. This decrease in the DM setting implies an increase in fork stalling caused by the inability to effectively

tolerate the high abundance of UV-C induced DNA lesions. In the WT setting, the increase in fork speed implies an increase in repriming.

If a system becomes reliant on repriming, single-strand gaps are expected to be generated. In DNA fibers, these ssDNA gaps can only be detected and quantified indirectly by an S1 nuclease treatment prior to spreading (Fig. 3C). Applying this approach, we observed a profound decrease in track length in the DM lymphoma, while WT cells remained unaffected under standard culture conditions (Fig. 3B). These findings indicate that the observed increase in fork speed likely relates to increased repriming. Upon UV-C exposure and S1 treatment, only WT cells displayed decreased track length as compared to non-UV-C exposed but S1 treated conditions, while the track length in DM cells remained the same (Fig. 3B). This implies that the increased replication speed in WT is based on increased repriming activity, which becomes necessary when challenged with exogenous replication stressors. In contrast, the DM system remains reliant on repriming in both unchallenged and challenged conditions (Fig. 3B), suggesting that DM predominantly use repriming as a mode DDT to alleviate replication stress [52].

Our results indicate that a CST deficiency in the DM did not result in a major defect in handling exogenous genotoxic stress but exerts its function primarily under specific endogenous stress conditions, as shown by cell cycle data (Fig. 2F). To study this more directly, we determined the consequences of a ST1 KO on replication fork speed under endogenous and exogenous replication stress conditions (Fig. 3D). Here, we took advantage of BCL2 overexpression to study the CST deficiency in the absence of a global DDT. Unexpectedly, BCL2 overexpression appeared to reduce the increased replication speed in the DM. In the absence of STN1, fork speed was found increased. Upon induction of UV lesions, the lack of a CST complex had no additional effects on top of what was observed in the DM (Fig. 3B, 3D). Using the S1 cleavage assay, we determined the extent of ssDNA in nascent DNA fibers in these cells (Fig. 3D). Remarkably, while BCL2 overexpression in the DM reduced the amount of ssDNA, the STN1 KO displayed a marked decrease in track length. This indicates a critical contribution of the CST complex in promoting fork stability and preventing the generation of ssDNA during replication under endogenous conditions. Again, upon UV-C exposure, there was no additional changes of a STN1 KO DM as compared to the phenotype of the BCL2 overexpressed DM control, suggesting that CST activity prefers specific types of lesions or impediments [53, 54].

DDT-deficient cells are prone to acquire large genomic deletions

To investigate the role of DDT in mutagenesis and genome maintenance, we performed WGS in DM lymphomas under endogenous and exogenous stress conditions. This was achieved by comparing two isogenic clones of both the WT and DM cells against a general reference genome (mm10). Subsequently, a comparison was made between the WT and DM cells themselves. Analyzing the large-scale mutations (structural variances), we observed a significant increase in deletions larger than 50 bp in the DM (Fig. 4A). No significant changes were detected in the other types of large-scale mutations such as large insertions or duplications, which in general are molecularly more complex and hence are less frequent mutational events. To examine the deletion landscape in

DDT-deficient cells in more detail, we plotted the size distribution of deletions and identified three distinct peaks of progressively larger deletion size (termed type 1, 2, and 3 deletions) (Fig. 4B). Importantly, type 3 deletions, ranging in size from 0.4 to 4.0 kbp, were found to be increased in DM cells compared to WT cells (Fig. 4B). To determine if the formation of these deletions could also be induced through exogenous lesions, we exposed the cells to UV-C irradiation. Compared to WT, the DM cells showed a specific increase in type 3 deletions upon UV-C (Fig. 4C). Notably, when UV exposed DMs were compared against non-treated DMs, we also saw a selective increase in these deletions, showing that these large deletions are damage-inducible in DDT deficient cells (Fig. 4D). Overlaying the total number of deletions in all conditions demonstrates a role of DDT in preventing type 3 deletions upon encountering exogenous lesions (Fig. 4E). No difference was observed in the genomic location of type 3 deletions seen between WT and DM cells untreated or treated with UV (Additional file 1: Fig. S5A and S5B). This argues against specific sites of genome that are more prone for type 3 deletions.

Given the recurrent, characteristic, multimodal size distribution of genomic deletions and that they likely require at least a single DSB [55], we hypothesized that each modus underlies a molecularly distinct DSB processing pathway. To approach this hypothesis, we examined the extent of microhomology at the junction sites of the deletions. Consistent with this concept, each peak displayed unique microhomology preferences at the break/junction sites (Fig. 4F, Additional file 1: Fig. S5C), suggesting that different molecular processes are involved in generating this characteristic size spectrum of genomic deletions. Type 1 deletions, ranging from 30 to 90 bp, displayed varied pattern of homology sizes with an increase in microhomology of 1–3 bps. Interestingly, the type 2 deletions ranging between 90 and 500 bp showed a very specific 14–17-bp microhomology preferences. Type 3 deletions, with the specific increase in the DDT-deficient cells, shows again an increase in microhomology of one and two base pairs under endogenous conditions. Unique about the homology pattern in the third peak was that the frequency of 1–2 bp microhomology was increased in the DM cells compared to the WT cells, whereas the homology pattern of all other base pairs was found non-significantly changed between genotypes (Fig. 4F). UV exposure only affected the homology pattern

(See figure on next page.)

Fig. 4 Whole-genome sequencing analysis of DDT deficient cells. **A** Number of structural variances found in WT and DM lymphomas. *P* values were determined using an unpaired Student *t*-test. **P* < 0.05. **B** (Left) Deletion size density plot of WT and DM lymphomas, average of two samples. (Right) Number of type 3 deletions found in WT and DM lymphomas. *P* values were determined using an unpaired Student *t*-test. ***P* < 0.005. **C** (Left) Deletion size density plot of deletions that occurred after the exposure of 0.4 J/m^2 UV-C of the WT and DM lymphomas, average of two samples. (Right) Number of type 3 deletions found in WT and DM lymphomas after UV-C exposure. *P* values were determined using an unpaired Student *t*-test. **P* < 0.05. **D** (Left) Deletion size density plot of deletions that occurred in untreated DM lymphomas compared to DM lymphomas after the exposure of 0.4 J/m.^{2} UV-C. Average of four samples in untreated conditions, average of two samples in UV-C treated conditions. (Right) Number of type 3 deletions found in WT and DM lymphomas under indicated conditions. *P* values were determined using an unpaired Student *t*-test. **P* < 0.05. **E** Deletion size density plot of deletions all deletions present in the cultured WT and DM cells and the UV exposed WT and DM cells with the different type of deletion ranges indicated. **F** Bar graph of the percentage of homology found at indicated types of deletion ranges of WT and DM lymphomas. *P* values were determined using multiple unpaired Student *t*-tests with two-stage step-up correction (Benjamini, Krieger, and Yekutieli). ** *q* < 0.005, *** *q* < 0.0005

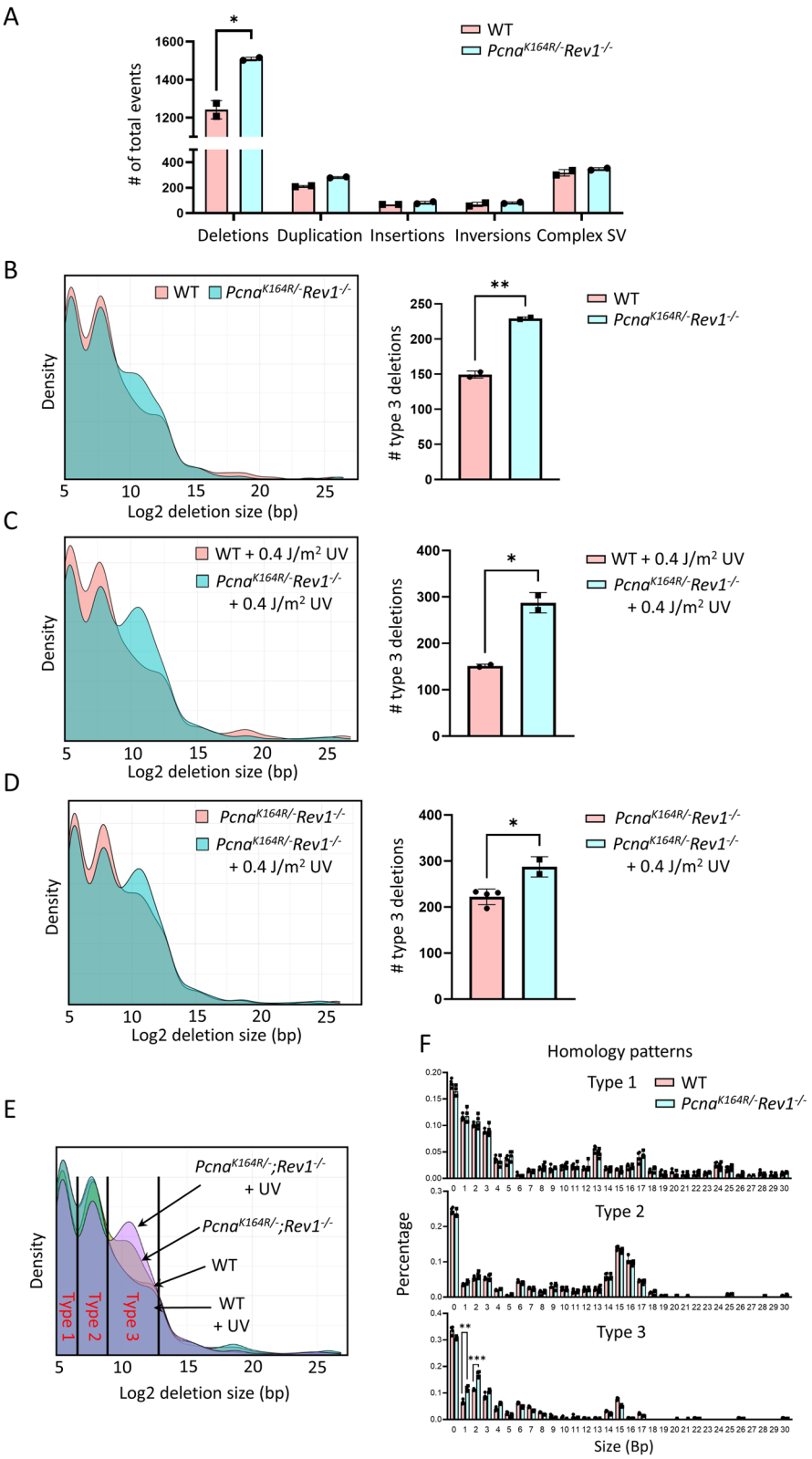

Fig. 4 (See legend on previous page.)

of type 3 deletions, where the DM cells had a significant increase in deletions with a microhomology signature of 3 bp compared to the non-treated DM cells (Additional file 1: Fig. S5A). These results support the concept that the multimodal size-distribution of genomic deletions underlies distinct molecular activities where DNA repair associated with type 3 deletions likely relates to one of the yet poorly defined A-EJ pathways. This argues against the involvement of canonical NHEJ, single-strand annealing (SSA), and HR generating type 3 deletions [56, 57]. Taken together, our results reveal that DDT prevents the accumulation of large genomic deletions in a DNA damage-dependent manner. These large deletions are likely repaired via a distinct, yet undefined, microhomology dependent A-EJ pathway [11].

Recently, Gyüre et al. generated and reported on a $PCNA^{K164R}$;$REV1^{-/-}$ double mutation in human TP53 deficient RPE-1 cells [58]. Among other findings, they reported the presence of large-scale deletions in their mutants. They also described the mutational effects of single mutants, including $REV1^{-/-}$ and $PCNA^{K164R}$, as well as other TLS proteins such as *REV3L* and *PRIMPOL*. Although they reported deletions of similar size in the DM system, they attributed these deletions to the *REV1* single mutant, where these deletions were also present. Conversely, the $PCNA^{K164R}$ mutant did not exhibit a similar deletion spectrum [58]. To compare these findings, we performed WGS of our single mutants and investigated the deletion spectrum (Additional file 1: Fig. S6). Neither of the single mutants displayed a significant difference in type 3 deletion numbers compared to WT controls. Likewise, exposure to UV-C also did not reveal any differences between the single mutants and WT cells.

Surprisingly, WGS results of $Pcna^{K164R/-}$;$Rev1^{-/-}$ cells failed to reveal small-scale mutations (Additional file 1: Fig. S7). These data indicated that the frequency and distribution of point mutations were highly comparable. Likewise, the frequency and distribution of InDels, and the mutational spectra were highly similar between the WT and DM clones (Additional file 1: Fig. S7B-E). As only the removal of DDT did not reveal any major differences in these types of small mutations, and as DDT is responsible for resolving different types of lesions, we examined how UV-C affected genomic stability of DDT-deficient cells. In line with the previous results, no differences were observed in substitutions and InDels (Additional file 1: Fig. S7). Furthermore, the single base pair substitution spectrum as described by Alexandrov et al. [59] failed to reveal significant changes in the type or quantity of point mutations. Despite the critical role of DDT in tolerating DNA lesions and other structural impediments during replication, our results argue that replicative bypass or persistent replication blockade in the absence of DDT does not result in major changes in small-scale mutations. Apparently, DDT plays a major role in alleviating replication-stress induced genome instability by preventing type 3 deletions, without introducing small-scale mutations.

Type 3 deletions can dominate the deletion landscape in human tumors

If conserved evolutionarily, it is expected to find a similar multimodal size distribution of genomic deletions in WGS samples of different species. To address this question and determine whether type 3 deletions arise in human cells as well, we took advantage of the publicly available WGS database from the Hartwig Medical Foundation (HMF). This

unique database contains more than 4500 human tumors. Random sampling of tumors and averaging the deletion size distributions revealed—except for type 2 deletions—a similar size distribution of human tumor samples and the mouse lymphoma (Fig. 5A). Deletions within the smallest range of size distributions (30–75 bp, type 1) occurred in both mouse and human tumors, whereas the type 2 deletions (120–360 bp) were only detected in the mouse lymphoma. Interestingly, a recurrent proportion of type 3 deletions (0.4–4.0 kbp) was present in most human tumor types (Fig. 5A). This recurrent multimodality suggests evolutionarily conserved molecular mechanisms underlying the size-restrictions of these deletions. Furthermore, when compared to randomly selected samples of the same tumor type, a subset of tumors was found highly enriched in type 3 deletions, indicating the existence of conditions favoring type 3 deletions in human tumors (Fig. 5A). To determine the frequency of human tumors containing type 3 deletions, we looked at the percentage of deletions that fall within the range of type 3 deletions compared to the total amount of deletions present. Consistently across different tumor types, 20 to 35% of tumors seem to contain 25% or more type 3 deletions (Fig. 5B). Taking this 25% cutoff and plotting the density profiles clearly indicated that the distribution of deletions favors a sizeable increase of type 3 deletions, independent of tumor origin (Fig. 5C).

DNA repair defects and activities correlate with the type 3 deletions in human tumors

There is a delicate balance between DNA repair activity and defects in determining whether mutations such as deletions are acquired. As replication stress can provoke DSBs which underly the formation of genomic deletions, we investigated the role of different DNA repair genes in the generation of type 3 deletions in human tumors. Tumors were stratified based on either a deletion or 20-fold amplification of known DNA repair genes. Tumors with the six most frequently amplified or deleted genes were compared (Fig. 5D). The combined density profiles of the deletion sizes of these tumors revealed a remarkable trend where the loss of DNA repair genes correlated with an increase in type 3 deletions, whereas an amplification of DNA repair genes led to their decrease (Fig. 5E, Additional file 1: Fig. S8A-B). As no specific relation was found between these genes and specific DNA repair pathways, distinct DDR defects are likely to enhance replication stress and DSBs, kick-starting the generation of type 3 deletions as well as others. The fact that except for type 2 deletions the deletion profiles between human tumors and mouse lymphomas appear similar, along with the reliance of these types of deletions on

(See figure on next page.)

Fig. 5 Analysis of large deletions in human tumors. **A** (Top) Combined deletion size density plot of 50 randomly selected human tumors of the indicated tumors type including WT and DM mouse lymphoma. (Bottom) Combined deletion size density plot of a selection of human tumors that are enriched in type 3 deletions of the indicated tumor type including WT and DM mouse lymphoma. **B** Frequency of tumors with the indicated percentage of all deletions being within 0.4–4 kbps. **C** Deletions size density plot of tumors with 25% of their deletions being within 0.4–4 kbps. **D** Scheme to investigate the effect of DNA repair gene proficiency on deletion sizes. Patients' tumors were selected with either a deletion or 20-fold amplification of listed DNA repair genes. The top 6 genes with the most tumors found with the indicated mutation are shown and used for the analysis. **E** Combined deletion size density plot of tumors with either an amplification or deletions in DNA repair genes or randomly selected tumors. **F** Deletion size density plots of tumors, regardless of tumor type, that received different types of treatments

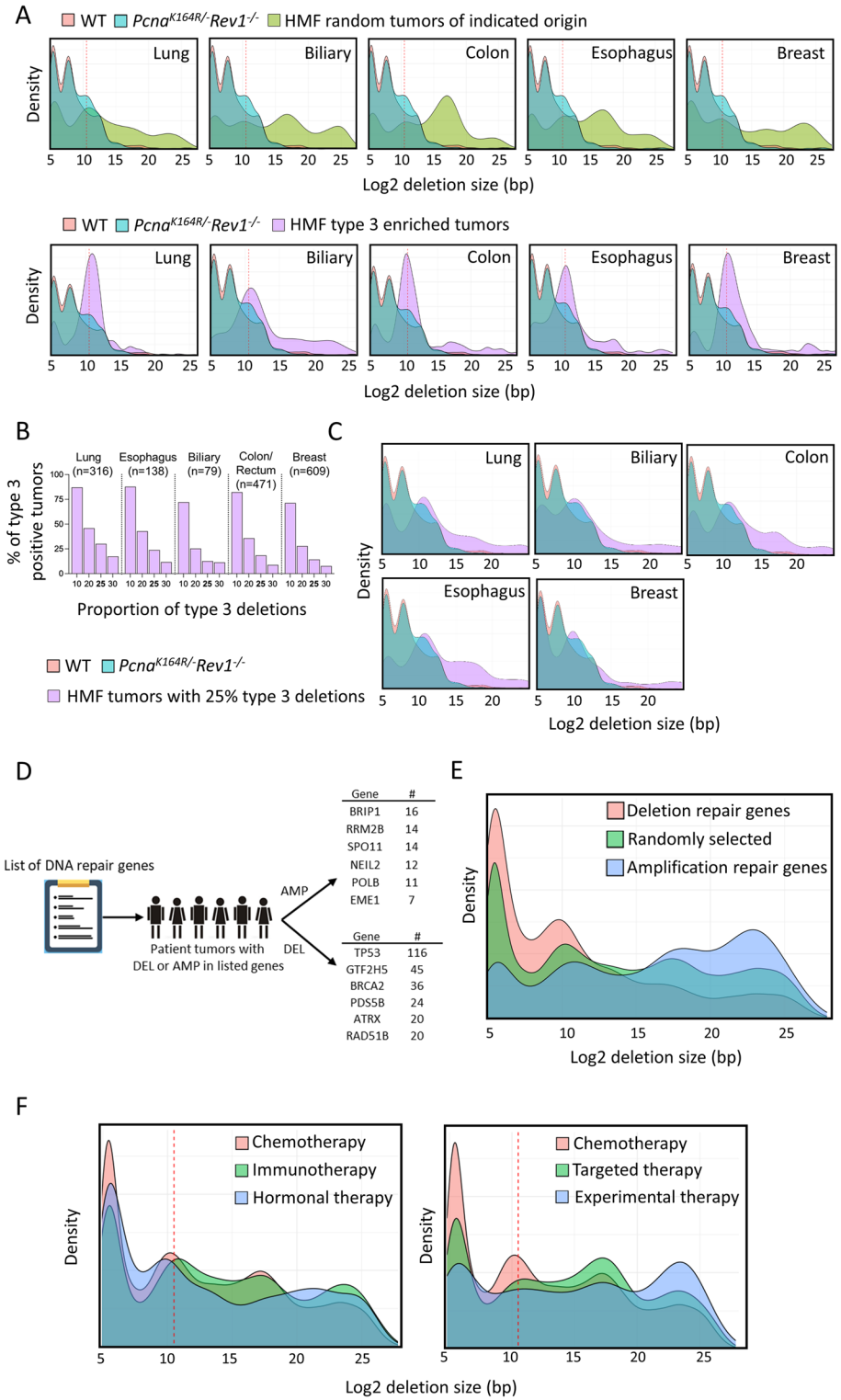

Fig. 5 (See legend on previous page.)

the proficiency of DNA repair genes in both species, implicates a conserved molecular mechanism and/or (epi)-genetic condition underlying the generation of type 3 deletions. Furthermore, comparing different therapies showed that the deletion spectra and

specifically the frequency of type 3 deletions are influenced by the treatment modality (Fig. 5F). A preference in the accumulation of type 3 deletions was found upon chemotherapy, immunotherapy, and hormonal therapy, while decreased in experimental and targeted therapy especially in tumors treated with tamoxifen, durvalumab, imatinib, or lorlatinib (Fig. 5F, Additional file 1: Fig. S9).

Discussion

Both PCNA-Ub and REV1 are critical components of the DDT system. Compound mutants lacking PCNA-Ub and REV1 were found synthetic and embryonic lethal (PNAS, Additional file 1: Fig. S1B). This synthetic lethality could be rescued by P53 downmodulation or inactivation. Taking advantage of this knowledge, we here investigated the molecular dependencies and genomic impact of a global DDT defect in the mammalian system. To eliminate the possibility of unintended genetic alterations due to off targeting of the CRISPR/Cas9, we employed an isogenic system and utilized two independent clones, both of which exhibited consistent phenotypes. Moreover, the utilization of a DM model has been extensively documented in previous independent studies, yielding results consistent with those observed in our study [26, 40, 58, 60]. As expected, DDT-deficient DM cells were hypersensitive to replication blocking lesions and in accordance displayed a marked increase in replication stress responses. Despite these impairments, the cell cycle remained largely unaffected under unperturbed conditions but with a noticeable increase of cells arrested in inter S phase. The fact that cells can survive in the absence of PCNA-Ub and REV1 dependent DDT suggest the existence of a compensatory DDT backup mode. To delineate the molecular dependencies of DM cells and gain deeper insights into how cancer cells, and to some extent normal tissue, can thrive in a DDT deficient environment, we conducted a comprehensive whole-genome CRISPR-Cas9 dropout screen. While the specific mutations observed in the DM cells are highly improbable to arise naturally, they provide a valuable model for replication stress, a condition that is very common in tumors [61]. This approach enabled us to identify key genetic factors and pathways that contribute to cell survival and proliferation in the absence of robust DDT mechanisms. Interestingly, the CST complex was identified as essential for DM cells. Moreover, as CST has been associated with replication, including fork stability, telomere maintenance, repriming via POLA, and tolerance of oxidative damage, as well as de novo origin firing, we characterized the contribution of CST in alleviating replication stress under compromised DDT conditions [41, 42, 47, 53, 54]. Further validation by a KO of STN1 (encoded by *Obfc1*) confirmed a vital dependence of DM cells on CST. To enable the investigation of a "dropped out" CST target complex, we first had to overexpress the antiapoptotic BCL2 by lentiviral transduction ensuring cell survival. In the absence of CST, DM lymphoma cells were found similarly sensitive to exogenous stressors as CST-proficient DM controls, whereas under non-challenged conditions, the cell cycle was severely affected. This argues against an important function of CST response to exogenous stressors, under DDT-deficient conditions. Instead, in the absence of DDT, CST appears primarily enrolled in processing endogenous lesions and other replication impediments such as oxidative damage, G4-stacks, hairpins, and Z-DNA structures [53].

As DDT is essential for mammalian replication and cell proliferation which can be rescued by p53 inactivation, we studied the effect of a DM on replication using the DNA fiber assay [51, 62, 63]. A global DDT defect resulted in a highly increased replication fork speed, which is consistent with a report on the impact of replication stress on fork speed and repriming [64, 65]. Indeed, as suggested by S1 nuclease digestion of nascent DNA fibers, repriming appears to predominate as a backup DDT mode to bypass lesions in the absence of PCNA-Ub and REV1 and prohibit cell death by prolonged fork stalling [52]. The replication fork dynamics of single mutants have been extensively studied by both us and others. Studies examining fork speed and repriming have consistently revealed no discernible impact of REV1 on either parameter [40, 66–72]. Additionally, our prior investigations have confirmed that the fork speed remains unaffected in PCNA K164R cells. Therefore, the effects observed in the current study appear to the result of the DM. Furthermore, UV-C exposure decreased the fork speed in the DM while increasing it in the WT. The increased fork speed in WT cells likely relates to repriming as revealed by the shortening of the track length upon S1 treatment. In line, the decreased fork speed in the DM is probably caused by increased fork stalling due to an impaired capacity to process the excessive number of lesions leading to an intra S phase arrest and cell death (Fig. 1C). The S1 data indicate that also under UV-C conditions DM cells rely on repriming to warrant fork progression.

Remarkably, as shown in Fig. 3D, overexpression of BCL2 in DM cells modulated DDR signaling such that besides a survival advantage, sufficient replication fidelity is gained to reduce repriming (Fig. 3D, right panel, light blue) and associated fork speed (Fig. 3D, left panel, light blue). In support of previous conclusion, STN1 KO had no effect other than those observed in the DM cells, when exposed to UV. This suggests that CST is primarily required in alleviating endogenous replication impediments. Interestingly, our STN1 KO data revealed an increased fork speed (Fig. 3D, right panel, light red) accompanied by increased repriming activity (Fig. 3D, right panel, light red), implicating that CST exhibits its contribution to DDT activity by stabilizing replication forks and prohibiting repriming. Given that DM cells already exhibit a high rate of repriming, failure to prohibit further repriming in DM cells lacking CST likely explains the dependence of DM on CST, i.e., DM cells must prevent extensive repriming to warrant survival. This interpretation is in line with the observation, that PrimPol, a potent primase at stalled forks, was not found in our drop out screen of DM lymphoma cell line [52, 73]. In this way, fork stabilization may facilitate an inefficient POLD/E polymerase switch to TLS polymerase by unmodified PCNA, as suggested previously [74, 75].

A central remaining question in the DDT field relates to the pro- and anti-mutagenic contribution of DDT pathways to genome maintenance. Applying WGS, we here identified a critical role of DDT in preventing the generation of damage-inducible large genomic deletions spanning between 0.4 and 4.0 kbp, which were also found in human tumors, which in general experience replication stress [61, 76]. Furthermore, breakpoint junction analysis revealed that the generation of these deletions prefers a 1 to 3 base pair microhomology. Notably, the size density profile of deletions in the mouse cells revealed a multimodal distribution defined as type 1, 2, and 3 deletions, characterized by specific size and microhomology preferences. The first type of deletions is reminiscent of the small deletions previously identified by TMEJ [77] and depend on single bp

microhomologies. In contrast to these type 1 deletions which occur in mice and humans, type 2 deletions were specific for the murine system. Type 2 deletions are characterized by unusual microhomology preference of 15 and 16 bp. Taken together, the discrete size preferences associated with distinct patterns of microhomology at the break-junction sites supports a concept where distinct molecular activities underlie the generation of these deletions. Furthermore, 5-month expansion of a DM clone and subsequent subcloning failed to reveal an increase in the number of type 3 deletions. Notably, these cells did not enter senescence but rather continued proliferation. In conjunction with the UV data, this observation implies that these deletions emerge predominantly during periods of heightened replication stress, indicating that they may serve as a hallmark of such conditions. Remarkably, no UV mutation signature was identified in either WT or DM cells following exposure to UV radiation, contrary to expectations [61, 76]. Despite the clear evidence of UV exposure indicated by the presence of deletions, we hypothesize that the absence of a UV mutation signature likely attributes to the low dose of UV-C administered to these cells. This cautious approach was necessary due to the heightened sensitivity of DM cells to UV radiation, rendering them incapable of surviving higher doses. While the usage of a general reference genome (mm10) for mutation calling, as employed in this study, is a common practice, it can lead to an increased presence of background mutations and may fail to filter out mutations shared with the ancestor cell line from which the WT and DM lines are derived. This could potentially account for the lack of disparity observed in small-scale mutations. However, it is worth noting that other studies in DDT-deficient systems have reported only low numbers of these mutations to begin with [4, 58, 69]. Nevertheless, it is important to emphasize that these considerations do not diminish the significance of the changes that were indeed detected, particularly the notable occurrences of large deletions.

The findings of Gyüre et al. strengthen the evidence that type 3 deletions are truly present in DDT deficient settings. However, some of their other findings deviate from ours, such as differences in the number of small deletions and their results in the single mutants. These differences could be attributed to the use of different cell systems (retinal pigment epithelial cells vs. thymic lymphoma) or species differences. Interestingly, in the HMF database, tumors with REV1 deletion/mutation did not show a particularly high number of deletions or type 3 deletions. While not all our findings corroborate those of Gyüre et al., the presence of the same deletions in the DM system strengthens the core of both studies. From the studies of Gyüre et al., it appears that the type 3 deletions are related to replication stress as imposed by a p53 deficiency. Future studies using other additional systems should reveal potential issues related to the origin of the cells and their DDR competency.

Interestingly and in line with these in vitro observations, our unbiased analyses of whole-genome sequences of human tumors revealed the presence of similar sized type 3 deletions. Type 3 deletions were highly abundant in all tumor types. Replication stress is a hallmark of tumors [61, 76], and in line with this notion, these type 3 deletions correlated with DNA repair status. Amplification of repair genes prevented type 3 deletions and inactivation of DNA repair genes favored their generation. Furthermore, the treatment modality of tumors was found to affect the deletion size spectrum independent of the tumor type. While the majority of these tumors did not exhibit specific defects

similar to our DM lymphomas, they unmistakably display a type 3 deletion phenotype. It is plausible that these tumors exhibit elevated replication stress, due to the lack of critical cell cycle check points, diminished DDR activity, and heightened incidence of replication stalling due to therapeutic interventions. This again implies that type 3 deletions represent a broader phenotype related to increased replication stress. Based on these findings, we favor a model where prolonged fork stalling leads to fork collapses and associated DSBs. Besides replication stress, deletion initiated by DSBs may also arise through other alterations in the DNA damage response network, suggesting DSBs as critical intermediate towards type 3 deletions. Alternatively, deletions may arise by looping of nonreplicated tracks of ssDNA independent of a DSB, as suggested recently [78]. Long tracks of single-stranded underreplicated DNA, spanning up to several kilo base pairs, were reported by Lopes et al. in yeast [19], correlating with the size of type 3 deletions, hinting that under-replication may underlie these deletions.

A recent report indicated that deficiencies of single TLS polymerases in *C. elegans* resulted in the formation of large 100–600 bp genomic deletions in a POLQ-dependent manner [79]. Though these deletions display both a different size and microhomology pattern, it argues in favor of DDT preventing large deletions in multiple phyla of life. Likewise, point mutagenesis in TLS-deficient animals was also not observed [79], in line with the absence of overt point mutagenesis in our lymphoma lines. Additionally, large deletions (> 50 bp) were detected in HSCs and p53-immortalized cells taken from *Fancd2*$^{-/-}$*Aldh2*$^{-/-}$ mice [4]. These findings are consistent with the concept where unresolved lesions, causing an increase in replication stress, can induce large deletions. The link between ICL repair and large deletions can give an explanation of the existence of type 3 deletions in human tumors, as these tumors frequently lose ICL repair and are often treated using DNA damaging agents [80]. Consequently, ICLs will accumulate leading to replication stress and DSBs that serve as possible substrates of type 3 deletions. This concept is supported by the result that chemotherapy favors type 3 deletions. Interestingly, the mutagenic signatures of primary and p53-immortalized *Fancd2*$^{-/-}$*Aldh2*$^{-/-}$ cells appear very similar [4], arguing against a general role of P53 on the mutagenic landscape and in extension in our experimental settings. Additionally, similar findings such as the absence of small-scale mutations and formation of large deletions in *C. elegans* [69], a non-transformed system, also oppose a direct role of P53 in the formation of these large deletions.

Conclusion

To conclude, this study firmly establishes a critical non-redundant contribution of PCNA-Ub and REV1 in DDT. An unbiased genome wide CRISPR screen identified the CST complex as essential back up in the absence of PCNA-Ub and REV1 facilitated DDT, where CST appears essential in preventing excessive repriming. Furthermore, we demonstrate that DDT exerts an anti-mutagenic function within the DDR network, by alleviating replication stress to protect the genome from structural variances. A multimodal size distribution of genomic deletions was observed. This multimodality is characterized by distinct MH signatures at the break ends. Our results indicate that DDT plays a critical role in preventing large deletions of the third modality, here classified as type 3 deletions. The multimodality likely reflects distinct stress conditions and repair

activities, where type 3 deletions are a signature of replication stress. Future work will have to delineate the molecular conditions and determinants underlying the deletion mechanisms.

Methods

Derivation of isogenic DDT proficient and deficient mouse thymic lymphoma cell lines

To obtain WT and $Pcna^{K164R/-}$;$Rev1^{-/-}$ lymphoma cell lines, 10×10^6 lymphoma cells from a p53-KO, $Pcna^{K164R/loxP}$ mouse [48] were nucleofected with the pX333 plasmid [81]. A nucleofector II-b device (Amaxa, Lonza), program A-30 with 10 μg of plasmid DNA and 1 μg of eGFP control plasmid (Amaxa, Lonza) was used. Subsequently, GFP or mCherry-positive cells were sorted with MoFlo Astrios or FACSAria IIu (BD Biosciences) cell sorters. Clones were obtained via limiting dilution. To obtain DM lymphoma cells, $Pcna^{K164R/-}$ mutant cells were transfected with the indicated guides against *Rev1* (Additional file 1: Fig. S1A).

Generation of mouse embryonic fibroblasts

Primary MEFs were isolated from E14.5 embryos intercrosses of $Pcna^{K164R/+}$;$Rev1^{+/-}$ and $Pcna^{K164R/+}$;$Rev1^{-/-}$ mice. Lentivirally transduction with p53 shRNA [82] was performed in order to immortalize the MEFs.

gRNA design to target murine *Pcna* and *Rev1*

Benchling was used to design guides targeting two exons or introns of each gene. For *Pcna*, the following guides were used: 5′-TAGTAAGGGGGCGTCCAGTT-3′ and 5′-GAATTTTGGACATGCTAGGG-3′. For *Rev1*, the same guides were chosen that had been used to generate the $Rev1^{-/-}$ mouse: 5′-AGAAATCTAATGATGTTGCATGG-3′, and 5′-TGAAGCACTGATTGACGTCACGG-3′. These were cloned into pX330 (one guide per plasmid) or a modified form of pX330, named pX333-mCherry, which contained sites for two guides. The protocol from Ran et al. was used to clone the guides in pX330 [83].

Isolation of genomic DNA and PCR

To obtain DNA for mouse-genotyping, and to screen for the presence of mutations in *Pcna*- or *Rev1* in lymphoma cells, cells or mouse toes were lysed with ProtK (10 mg/mL). Mutations were screened for using PCR (see Additional file 1: Table S1 for primers and Table S2 for PCR settings).

Proliferation assay MEFs

Viable primary MEFs or p53kd MEFs were seeded at the concentration of 300 cells per well in 96-well plates. The cells were allowed to grow for 8 days or 10 days in IncuCyte® (Essenbioscience) under standard tissue culture conditions. Images were taken every 4 h, and results were analyzed in Excel (Microsoft) as percentage of confluence that represents the percentage of the image area occupied by objects.

Survival assay, synergy experiments, and high-throughput compound screen

For survival assays in the lymphoma cell lines, cells were seeded at low confluency using the Multidrop Combi (Thermo Fisher Scientific), into 384-well plates (Greiner). After 24 h, the respective compounds were added using a tecan d300e compound printer (HP), including 3–5 replicates per dosage. Positive (1 μM phenylarsine oxide) and negative (0.1% DMSO) controls were added to each assay plate. Viability readout was performed after 72 h, using the CellTiter-Blue assay (G8081/2, Promega) following the protocol of the manufacturer using an EnVision multimode plate reader (PerkinElmer). The CTB data was normalized per plate using the normalized percentage inhibition (NPI) method [84]. NPI sets the mean of the positive control value to 0 and mean of the negative control to 1. Synergy calculations were performed in R using the Chou-Talalay Combination index method cytometry. UV survival assays were performed by seeding 500,000 cells in 24-well plates and treated with UV-C. After 72 h, viability was assessed by flow cytometry. For the high-throughput drug screen in lymphoma cells, the following procedure was followed: using the Multidrop Combi (Thermo Fisher Scientific), untreated p53-KO lymphoma cells were seeded into 384-well plates at low confluency. After 24 h, the collection of compound libraries available at the NKI (Selleck GPCR, Kinase, Apoptosis, Phospatase, Epigenetic, LOPAC, and NCI oncology) was added. This library was stored and handled as recommended by the manufacturer. Compounds from the master plate were diluted in daughter plates containing complete RPMI 1640 medium, using the microlab star liquid handling workstation (Hamilton). From the daughter plates, the diluted compounds were transferred into 384-well assay plates, in triplicate, with final concentrations of 1 μM and 5 μM. In addition, positive (1 μM phenylarsine oxide) and negative (0.1% DMSO) controls were added alternately to wells in columns 2 and 23 of each assay plate. After 3 days, viability was measured using CellTiter-Blue assay (G8081/2, Promega) following the protocol of the manufacturer. The CTB data was normalized per plate using the normalized percentage inhibition (NPI) method. NPI sets the mean of the positive control value to 0 and mean of the negative control to 1. Using the replicate values of both conditions, a two-sided *t*-test was performed. Afterwards, the *P*-values were corrected for multiple testing using the Benjamini–Hochberg method. All calculations were done in R.

Measure of replication stress by yH2AX

Lymphomas were plated in 24-well plates with 500,000 cells per mL in 0.5 mL medium. After 15 min, cells were exposed to 20 J/m^2 UV-C and given 0.5 mL of fresh medium. To distinguish dead cells, cells were stained with LIVE/DEAD Fixable Yellow Dead Cell Stain Kit (Thermo Fisher) for 20 min. After this, cells were incubated at 37 °C for 4 h after which they were fixed and permeabilized with the Transcription Factor Buffer Set from BD. γH2AX was detected with PerCP/Cyanine5.5 anti-H2A.X-Phosphorylated (Ser139, clone 2F3, Biolegend) antibody (1:500). Finally, cells were resuspended in PBS with 7 μg/mL DAPI and measured on an Attune (Thermo Fisher). Data were analyzed using the FlowJo software version 10.7.0.

EdU incorporation assay

Cells were labeled with 1:1000, 10 mM EdU in regular medium for 20 min after which cell were washed, resuspended in PBS, and fixed in 100% ethanol. The Click-iT Plus EdU Flow Cytometry Kit AF488 (Thermo Fisher Scientific) protocol was followed. Cells were suspended in PBS containing 7 μg/mL DAPI to visualize DNA content. Finally, samples were measured with an Attune (Thermo Fisher) and analyses were performed using FlowJo version 10.7.0.

Whole-genome dropout screen

The Mouse Improved Genome-wide Knockout CRISPR Library v2 (Addgene #67,988) collection sgRNAs in lentiviral vectors targeting 18,424 mouse genes, with four to five individual sgRNAs for each gene, was used to infect WT and PcnaK164RRev1 -/- lymphoma with a 100-fold coverage. Lymphoma were harvested at $T=0$ after a 3-day period in which cultures underwent selection with 2 μg/mL puromycin to select for cells that had been transduced with the library. Cells were subsequently cultured for $\approx$ 10 cell divisions. After 10 doublings, gDNA was isolated using the DNAeasy blood and tissue kit (QIAGEN) following the manufacturer's protocol. For each line, one replicate was taken at $T=0$, and three replicates were taken at $T=10$. A capture protocol was performed to enrich for sgRNA sequences. gDNA was digested overnight at 37 °C with NdeI and XhoI. The following day, samples were heated for 10 min at 100 °C and subsequently snap frozen. After light thawing, biotinylated capture oligos were added to enrich for sgRNA-barcodes: NdeI-Fwd: 5′-TGCTTACCGTAACTTGAAAGTATTTCG ATTTCTTGGCTTTATATATCTTG-3′ and XhoI-Rev: 5′-GATCTAGATGGATGC AGGTCAAAGGCCCGGACATGAGGAAGAGGAGAA-3′. Samples were hybridized overnight at 60 °C. Biotinylated primers were captured using Streptavidin T1 dynabeads for 2 h at room temperature. After multiple washes, beads were used as input material for subsequent PCRs: sgRNAs were retrieved using Phusion High-Fidelity DNA Polymerase (Thermo Fisher Scientific) by a 2-step PCR protocol. First, biotinylated capture oligos were amplified in the first round of PCR amplification with 10 μL 5 × GC buffer, 1 μL 10 mM dNTP, 2.5 μL 10 μM PCR 1 indexed forward primer (Table S2, primers TRC_ PCR1_Fwd1-8, which contain the barcode to label each sample), 2.5 μL 10 μM PCR 1 indexed reverse primer (Table S2, primer Yusa_Rv_1st PCR), 1.5 μL DMSO, 1 U Phusion Polymerase, and H_2O added up to 50 μL and run at (1) 98 °C, 30 s; (2) 98 °C, 30 s; (3) 60 °C, 30 s; (4) 72 °C, 1 min (steps 2, 3, and 4 for 20 times), and 72 °C, 5 min. The product of PCR1 was used to setup the second PCR reaction similar to PCR1. In PCR2, primers containing P5 and P7 sequences were used. The abundance of the guide RNAs in the $T=0$ and T10 replicates was determined by Illumina Next Generation Sequencing. For the analysis of the screen, a differential analysis on the sgRNA level with DESeq2 was performed63. As hits, we selected genes for which at least two sgRNAs had a log2 fold change smaller than -1 and a FDR ≤ 0.1.

Sample preparation and immunoblotting

To validate the genetic ablation of STN1, lymphoma cells were lysed in RIPA buffer (25 mM Tris HCl (pH 7.6), 150 mM NaCl, 1% NP-40, 1% sodium deoxycholate, and 0.1% SDS) containing 1 × protease inhibitor cocktail (Roche) for 30 min on ice. Lysates were

sonicated for 15 min using a BioRuptor (30 s on, 30 s off, maximum power, at 4 °C). Samples were spun at 20,000 g for 10 min, and the protein concentration was measured either via the Bradford assay, or via a BCA assay. Samples were run on a 4–12% Bis–Tris gel with MES running buffer on ice, at 150–200 V for 1.5–2 h, until the loading band ran off the gel. Following, an overnight wet transfer was used. After staining with Ponceau-S, samples were blocked for 1 h using PBST containing 5% skim-milk powder, followed by incubation with primary antibodies *Obfc1* Ab (sc-376450 1:250) for 3 h at room temperature in TBS-T 1% milk. Blots were washed 3 times for 10 min with PBST, followed by a secondary staining (IRDye800CW goat anti-mouse, 1:5000 in PBST) for 1 h at room temperature. The membrane was washed 3 times with PBST for 10 min, after which the membrane was imaged on an Oddyssey scanner (LiCor). For loading control, GAPDH (14C10) was used (1:5000) as primary and IRDye680RD goat anti-rabbit (1:10,000) as secondary.

DNA fiber and S1 nuclease assay

In a 24-well plate, 300,000 cells were plated in 250 µL medium. Prior to UV-C exposure (20 J/m^2), lymphomas were incubated in medium containing 25 µM 5-chloro-2-deoxyuridine (CldU) for 20 min at 37 °C. After UV-C exposure, medium containing 500 µM 5-Iodo-2-deoxyuridine (IdU) was added, resulting in a final concentration of 250 µM IdU and 12.5 M CldU. After 60 min at 37 °C, 10 mL of 4 °C PBS was added, and cells were spun down at 1200 rpm for 5 min and resuspended in 1 mL PBS with 1% FCS. Two microliters of a suspension of 3×10^5 lymphomas per mL was spotted onto a microscope slide, incubated for 5 min and lysed with 7 µL lysis buffer (200 mM Tris–HCl pH7.4, 50 mM EDTA, 0.5% SDS) for 3 min. Slides were tilted to 15 °C to allow the DNA to run down the slide. Next, the slides were air dried and subsequently mixed in methanol-acetic acid (3:1). After rehydration, fixed DNA fibers were denatured in 2.5 M HCl for 75 min. Incorporation of CldU was detected using rat-anti-BrdU antibodies (1:500; BU1/75, AbD Serotec) and Alexa fluor-555-labeled goat-anti-rat antibodies (1:500; Molecular Probes), whereas incorporated IdU was detected using mouse-anti-BrdU antibodies (1:750; Clone B44, BD) and Alexa fluor-488-labeled goat-anti-mouse antibodies (1:500; Molecular Probes). Finally, slides were mounted in Fluoro-Gel (Electron Microscopy Sciences). Microscopy was performed using a fluorescent microscope (Zeiss). For the S1, nuclease assay cells were permeabilized with NuEX buffer after the staining and spinning. Next, cells were washed with S1 nuclease buffer and spun down at 7000 rpm for 5 min; 20 U/mL S1 in S1 buffer was added for 30 min at 37 °C, after which cells where washed and resuspended in 1 mL PBS with 1% FCS. The following steps were performed normally.

Whole-genome sequencing, mutation calling, and analysis

WT and DM lymphoma cells were either irradiated one time with UV-C (0.4 J/m^2) or left untreated. After, cells were left to recover for 3 days in regular medium; clones were obtained via limiting dilution. DNA was isolated using the Isolate II Genomic DNA kit (Bioline). Library preparation and whole-genome sequencing was performed at the Hartwig Medical Foundation using the HiSeqX system generating 2×150 base read

pairs. Sequencing quality control was done with FASTQC, followed by aligning by BWA [85] using the mm10 genome as reference. Finally, Mark Duplicates by Picard was used to remove duplicated reads. For structural variant calling, GRIDSS [86] (version 2.1.0–0) was used, and for small-scale mutations, GATK Haplotypecaller [87] (version 4.2.3.0) was used. Downstream analysis, quantification, and visualization was done in R (version 4.2.0). MutationalPatterns (version 3.6.0) package was used for generating the base substitution signatures plots.

Analysis of human whole-genome sequencing data

The Hartwig Medical Foundation [88] database containing > 4000 whole-genome sequenced human tumors was used for these analyses. For downstream quantification and visualization, R was used.

Statistical analysis

To assess the statistical significance of our data, we used the *t*-test, multiple unpaired Student *t*-test with two-stage step-up correction (Benjamini, Krieger, and Yekutieli), one-way ANOVA, or Mann–Whitney *U* test ($^{*}P < 0.05$, $^{**}P < 0.01$, $^{***}P < 0.001$, $^{****}P < 0.0001$) by GraphPad Prism 6 or 9. No statistical methods were used to predetermine sample size.

Supplementary Information

The online version contains supplementary material available at https://doi.org/10.1186/s13059-024-03451-z.

Additional File 1: Fig. S1. Generation of lymphoma cell line and survival of DDT deficient primary mouse embryonic fibroblasts. Fig. S2. Overview of compound screen. Fig. S3. Gating strategy of γH2AX and EdU assays. Fig. S4. Quality control of CRISPR screen and gating strategy STN1 KO lymphoma and control. Fig. S5. Type 3 location and microhomology signature after UV exposure. Fig. S6. Number of type 3 deletions in single mutants, with and without UV. Left graph: the PcnaK164R/- single mutant. Right graph: the Rev1-/- single mutant. Fig. S7. Analysis of small-scale mutations in WT and DM lymphoma. Fig. S8. Individual density plots of the deletion sizes of human tumors with an amplification or deletion in DNA repair genes. Fig. S9. Effect of specific treatment on deletion sizes. Table S1. Primer information and PCR settings.

Additional File 2: Review history at *Genome Biology*.

Acknowledgements
The authors wish to acknowledge R. Bin Ali from the Mouse Clinic for Cancer and Aging research (MCCA) Transgenic Facility for his help in generating Rev1$^{-/-}$ mouse and Roel of Pruntel for sequencing,

Peer review information
Andrew Cosgrove was the primary editor of this article at *Genome Biology* and managed its editorial process and peer review in collaboration with the rest of the editorial team.

Review history
This article was first peer-reviewed at Review Commons and reviewer reports are available online [89–91]. The authors' response to these reviews is available at [92]. The rest of the review history containing the authors' responses and additional reviewer comments are available as Additional File 2.

Authors' contributions
DdG, AS, RS, CL, RLB, and HJ designed the study and interpreted the results. DdG, AS, RS, MK, BM, PCMvdB, OAB, BP, SO, JJIC, MA, and CL performed experiments. DdG, AS, and HJ wrote the manuscript. HJ wrote the projects.

Funding
This work was supported by grants from the Dutch Cancer Society (KWF) to H. Jacobs (KWF NKI-2016–10032, and KWF NKI-2017–10796).
KWF Kankerbestrijding,10796,Heinz Jacobs,10032,Heinz Jacobs

Data availability
Custom R scripts that have been used to generate the figures are freely available at GitHub repository and Zenodo under the license CC BY-ND 4.0 [93, 94].

The WGS datasets generated during this study are available as a bioproject with the accession number PRJNA1017351 (https://www.ncbi.nlm.nih.gov/bioproject/PRJNA1017351) [95].
WGS data from human tumors are available through the Hartwig Medical Foundation at https://www.hartwigmedicalfoundation.nl/en/data/data-access-request/ [96]. The entire dataset as of 2023 was used.

Declarations

Ethics approval and consent to participate
Not applicable.

Consent for publication
Not applicable.

Competing interests
The authors declare that they have no competing interests.

Received: 22 February 2024 Accepted: 29 November 2024
Published online: 31 December 2024

References

1. Schumacher B, Pothof J, Vijg J, Hoeijmakers JHJ. The central role of DNA damage in the ageing process. Nature. 2021;592:695–703.
2. Rossi DJ, Bryder D, Seita J, Nussenzweig A, Hoeijmakers J, Weissman IL. Deficiencies in DNA damage repair limit the function of haematopoietic stem cells with age. Nature. 2007;447:725–9.
3. Tubbs A, Nussenzweig A. Endogenous DNA damage as a source of genomic instability in cancer. Cell. 2017;168:644–56.
4. Garaycoechea JI, Crossan GP, Langevin F, Mulderrig L, Louzada S, Yang F, Guilbaud G, Park N, Roerink S, Nik-Zainal S, et al. Alcohol and endogenous aldehydes damage chromosomes and mutate stem cells. Nature. 2018;553:171–7.
5. Biertümpfel C, Zhao Y, Kondo Y, Ramón-Maiques S, Gregory M, Lee JY, Masutani C, Lehmann AR, Hanaoka F, Yang W. Structure and mechanism of human DNA polymerase eta. Nature. 2010;465:1044–8.
6. Wu RA, Semlow DR, Kamimae-Lanning AN, Kochenova OV, Chistol G, Hodskinson MR, Amunugama R, Sparks JL, Wang M, Deng L, et al. TRAIP is a master regulator of DNA interstrand crosslink repair. Nature. 2019;567:267–72.
7. Pilzecker B, Buoninfante OA, Van Den Berk P, Lancini C, Song JY, Citterio E, Jacobs H. DNA damage tolerance in hematopoietic stem and progenitor cells in mice. Proc Natl Acad Sci U S A. 2017;114:E6875–83.
8. Tomas-Roca L, Tsaalbi-Shtylik A, Jansen JG, Singh MK, Epstein JA, Altunoglu U, Verzijl H, Soria L, van Beusekom E, Roscioli T, et al. De novo mutations in PLXND1 and REV3L cause Möbius syndrome. Nat Commun. 2015;6:7199.
9. Friedberg EC. Suffering in silence: the tolerance of DNA damage. Nat Rev Mol Cell Biol. 2005;6:943–53.
10. Gao Y, Mutter-Rottmayer E, Greenwalt AM, Goldfarb D, Yan F, Yang Y, Martinez-Chacin RC, Pearce KH, Tateishi S, Major MB, et al. A neomorphic cancer cell-specific role of MAGE-A4 in trans-lesion synthesis. Nat Commun. 2016;7:12105.
11. Chang HHY, Pannunzio NR, Adachi N, Lieber MR. Non-homologous DNA end joining and alternative pathways to double-strand break repair. Nat Rev Mol Cell Biol. 2017;18:495–506.
12. Mcculloch SD, Kunkel TA. The fidelity of DNA synthesis by eukaryotic replicative and translesion synthesis polymerases. Cell Res. 2008;18:148–61.
13. Wu W-J, Yang W, Tsai M-D. How DNA polymerases catalyse replication and repair with contrasting fidelity. Nat Rev Chem. 2017;1:1–16.
14. Pilzecker B, Buoninfante OA, Pritchard C, Blomberg OS, Huijbers IJ, van den Berk PCM, Jacobs H. PrimPol prevents APOBEC/AID family mediated DNA mutagenesis. Nucleic Acids Res. 2016;44:4734–44.
15. Knipscheer P, Enoiu M, Angelov T, Sun J, Griffith JD, Walter JC, Ellenberger TE, Scha OD. Mechanism of replication-coupled DNA interstrand crosslink repair. Cell. 2008;134:969–80.
16. Budzowska M, Graham TG, Sobeck A, Waga S, Walter JC. Regulation of the Rev1–pol ζ complex during bypass of a DNA interstrand cross-link. EMBO J. 2015;34:1971–85.
17. Ogi T, Limsirichaikul S, Overmeer RM, Volker M, Takenaka K, Cloney R, Nakazawa Y, Niimi A, Miki Y, Jaspers NG, et al. Three DNA polymerases, recruited by different mechanisms, carry out NER repair synthesis in human cells. Mol Cell. 2010;37:714–27.
18. Pilzecker B, Buoninfante OA, Jacobs H. DNA damage tolerance in stem cells, ageing, mutagenesis, disease and cancer therapy. Nucleic Acids Res. 2019;47:7163–81.
19. Lopes M, Foiani M, Sogo JM. Multiple mechanisms control chromosome integrity after replication fork uncoupling and restart at irreparable UV lesions. Mol Cell. 2006;21:15–27.
20. Hashimoto Y, Ray Chaudhuri A, Lopes M, Costanzo V. Rad51 protects nascent DNA from Mre11-dependent degradation and promotes continuous DNA synthesis. Nat Struct Mol Biol. 2010;17:1305–11.
21. Branzei D, Vanoli F, Foiani M. SUMOylation regulates Rad18-mediated template switch. Nature. 2008;456:915–20.
22. Sale JE, Lehmann AR, Woodgate R. Y-family DNA polymerases and their role in tolerance of cellular DNA damage. Nat Rev Mol Cell Biol. 2012;13:141–52.
23. Wit N, Buoninfante OA, van den Berk PCM, Jansen JG, Hogenbirk MA, de Wind N, Jacobs H. Roles of PCNA ubiquitination and TLS polymerases κ and η in the bypass of methyl methanesulfonate-induced DNA damage. Nucleic Acids Res. 2015;43:282–94.
24. Daigaku Y, Davies AA, Ulrich HD. Ubiquitin-dependent DNA damage bypass is separable from genome replication. Nature. 2010;465:951–5.

25. Vujanovic M, Krietsch J, Raso MC, Terraneo N, Zellweger R, Schmid JA, Taglialatela A, Huang J-W, Holland CL, Zwicky K, et al. Replication fork slowing and reversal upon DNA damage require PCNA polyubiquitination and ZRANB3 DNA translocase activity. Mol Cell. 2017;67:882-890.e5.
26. Edmunds CE, Simpson LJ, Sale JE. PCNA ubiquitination and REV1 define temporally distinct mechanisms for controlling translesion synthesis in the avian cell line DT40. Mol Cell. 2008;30:519–29.
27. Ross AL, Simpson LJ, Sale JE. Vertebrate DNA damage tolerance requires the C-terminus but not BRCT or transferase domains of REV1. Nucleic Acids Res. 2005;33:1280–9.
28. Guo C, Fischhaber PL, Luk-Paszyc MJ, Masuda Y, Zhou J, Kamiya K, Kisker C, Friedberg EC. Mouse Rev1 protein interacts with multiple DNA polymerases involved in translesion DNA synthesis. EMBO J. 2003;22:6621–30.
29. Quinet A, Martins DJ, Vessoni AT, Biard D, Sarasin A, Stary A, Menck CFM. Translesion synthesis mechanisms depend on the nature of DNA damage in UV-irradiated human cells. Nucleic Acids Res. 2016;44:5717–31.
30. Mailand N, Gibbs-Seymour I, Bekker-Jensen S. Regulation of PCNA–protein interactions for genome stability. Nat Rev Mol Cell Biol. 2013;14:269–82.
31. Yang W, Gao Y. Translesion and repair DNA polymerases: diverse structure and mechanism. Annu Rev Biochem. 2018;87:239–61.
32. Goodman MF, Woodgate R. Translesion DNA polymerases. Cold Spring Harb Perspect Biol. 2013;5: a010363.
33. Weaver TM, Click TH, Khoang TH, Todd Washington M, Agarwal PK, Freudenthal BD. Mechanism of nucleotide discrimination by the translesion synthesis polymerase Rev1. Nat Commun. 2022;13:2876.
34. Hodskinson MR, Bolner A, Sato K, Kamimae-Lanning AN, Rooijers K, Witte M, Mahesh M, Silhan J, Petek M, Williams DM, et al. Alcohol-derived DNA crosslinks are repaired by two distinct mechanisms. Nature. 2020;579:603–8.
35. Martín-Pardillos A, Tsaalbi-Shtylik A, Chen S, Lazare S, van Os RP, Dethmers-Ausema A, Fakouri NB, Bosshard M, Aprigliano R, van Loon B, et al. Genomic and functional integrity of the hematopoietic system requires tolerance of oxidative DNA lesions. Blood. 2017;130:1523–34.
36. Avkin S, Sevilya Z, Toube L, Geacintov N, Chaney SG, Oren M, Livneh Z. p53 and p21 regulate error-prone DNA repair to yield a lower mutation load. Mol Cell. 2006;22:407–13.
37. Silverstein TD, Johnson RE, Jain R, Prakash L, Prakash S, Aggarwal AK. Structural basis for the suppression of skin cancers by DNA polymerase η. Nature. 2010;465:1039–43.
38. Spanjaard A, Shah R, de Groot D, Buoninfante OA, Morris B, Lieftink C, Pritchard C, Zürcher LM, Ormel S, Catsman JJI, et al. Division of labor within the DNA damage tolerance system reveals non-epistatic and clinically actionable targets for precision cancer medicine. Nucleic Acids Res. 2022;50:7420–35.
39. Langerak P, Nygren AOH, Krijger PHL, van den Berk PCM, Jacobs H. A/T mutagenesis in hypermutated immunoglobulin genes strongly depends on PCNAK164 modification. J Exp Med. 2007;204:1989–98.
40. Buoninfante OA, Pilzecker B, Spanjaard A, de Groot D, Prekovic S, Song J-Y, Lieftink C, Ayidah M, Pritchard CEJ, Vivié J, et al. Mammalian life depends on two distinct pathways of DNA damage tolerance. Proc Natl Acad Sci U S A. 2023;120: e2216055120.
41. Rice C, Skordalakes E. Structure and function of the telomeric CST complex. Comput Struct Biotechnol J. 2016;14:161–7.
42. Barazas M, Annunziato S, Pettitt SJ, de Krijger I, Ghezraoui H, Roobol SJ, Lutz C, Frankum J, Song FF, Brough R, et al. The CST complex mediates end protection at double-strand breaks and promotes PARP inhibitor sensitivity in BRCA1-deficient cells. Cell Rep. 2018;23:2107–18.
43. Lyu X, Lei K-H, Biak Sang P, Shiva O, Chastain M, Chi P, Chai W. Human CST complex protects stalled replication forks by directly blocking MRE11 degradation of nascent-strand DNA. EMBO J. 2021;40: e103654.
44. Nguyen DD, Kim E, Le NT, Ding X, Jaiswal RK, Kostlan RJ, Nguyen TNT, Shiva O, Le MT, Chai W. Deficiency in mammalian STN1 promotes colon cancer development via inhibiting DNA repair. Sci Adv. 2023;9:eadd8023.
45. Hara T, Nakaoka H, Miyoshi T, Ishikawa F. The CST complex facilitates cell survival under oxidative genotoxic stress. PLoS ONE. 2023;18: e0289304.
46. Gasparayan H, Caridi C, Julius J, Feng W, Bachant J, Nugent CI. Yeast Stn1 promotes MCM to circumvent Rad53 control of the S phase checkpoint. Curr Genet. 2022;68:165–79.
47. He Q, Lin X, Chavez BL, Agrawal S, Lusk BL, Lim CJ. Structures of the human CST-Polα–primase complex bound to telomere templates. Nature. 2022;608:826–32.
48. Buoninfante OA, Pilzecker B, Aslam MA, Zavrakidis I, van der Wiel R, van de Ven M, van den Berk PCM, Jacobs H. Precision cancer therapy: profiting from tumor specific defects in the DNA damage tolerance system. Oncotarget. 2018;9:18832–43.
49. Tsuda M, Terada K, Ooka M, Kobayashi K, Sasanuma H, Fujisawa R, Tsurimoto T, Yamamoto J, Iwai S, Kadoda K, et al. The dominant role of proofreading exonuclease activity of replicative polymerase ε in cellular tolerance to cytarabine (Ara-C). Oncotarget. 2017;8:33457–74.
50. Tzelepis K, Koike-Yusa H, De Braekeleer E, Li Y, Metzakopian E, Dovey OM, Mupo A, Grinkevich V, Li M, Mazan M, et al. A CRISPR dropout screen identifies genetic vulnerabilities and therapeutic targets in acute myeloid leukemia. Cell Rep. 2016;17:1193–205.
51. Quinet A, Carvajal-Maldonado D, Lemacon D, Vindigni A. DNA fiber analysis: mind the gap! 1st ed. Elsevier Inc. 2017.
52. Pilzecker B, Jacobs H. Mutating for Good: DNA Damage Responses During Somatic Hypermutation. Front Immunol. 2019;10:438. https://doi.org/10.3389/fimmu.2019.00438.
53. Zhang M, Wang B, Li T, Liu R, Xiao Y, Geng X, Li G, Liu Q, Price CM, Liu Y, et al. Mammalian CST averts replication failure by preventing G-quadruplex accumulation. Nucleic Acids Res. 2019;47:5243–59.
54. Stewart JA, Wang Y, Ackerson SM, Schuck PL. Emerging roles of CST in maintaining genome stability and human disease. Front Biosci Landmark Ed. 2018;23:1564–86.
55. Klug WS, Cummings MR, Spencer CA, Palladino MA. Concepts of genetics. Eleventh. Boston: Pearson; 2015.
56. Scully R, Panday A, Elango R, Willis NA. DNA double-strand break repair-pathway choice in somatic mammalian cells. Nat Rev Mol Cell Biol. 2019;20:698–714.
57. Chapman JR, Taylor MRG, Boulton SJ. Playing the end game: DNA double-strand break repair pathway choice. Mol Cell. 2012;47:497–510.

58. Gyüre Z, Póti Á, Németh E, Szikriszt B, Lózsa R, Krawczyk M, Richardson AL, Szüts D. Spontaneous mutagenesis in human cells is controlled by REV1-Polymerase ζ and PRIMPOL. Cell Rep. 2023;42: 112887.
59. Alexandrov LB, Kim J, Haradhvala NJ, Huang MN, Tian Ng AW, Wu Y, Boot A, Covington KR, Gordenin DA, Bergstrom EN, et al. The repertoire of mutational signatures in human cancer. Nature. 2020;578:94–101.
60. Arakawa H, Moldovan G-L, Saribasak H, Saribasak NN, Jentsch S, Buerstedde J-M. A role for PCNA ubiquitination in immunoglobulin hypermutation. PLoS Biol. 2006;4: e366.
61. Gaillard H, García-Muse T, Aguilera A. Replication stress and cancer. Nat Rev Cancer. 2015;15:276–89.
62. Bensimon A, Simon A, Chiffaudel A, Croquette V, Heslot F, Bensimon D. Alignment and sensitive detection of DNA by a moving interface. Science. 1994;265:2096–8.
63. Parra I, Windle B. High resolution visual mapping of stretched DNA by fluorescent hybridization. Nat Genet. 1993;5:17–21.
64. Jacobs K, Doerdelmann C, Krietsch J, González-Acosta D, Mathis N, Kushinsky S, Guarino E, Gómez-Escolar C, Martinez D, Schmid JA, et al. Stress-triggered hematopoietic stem cell proliferation relies on PrimPol-mediated repriming. Mol Cell. 2022;82:4176-4188.e8.
65. Bainbridge LJ, Teague R, Doherty AJ. Repriming DNA synthesis: an intrinsic restart pathway that maintains efficient genome replication. Nucleic Acids Res. 2021;49:4831–47.
66. Muramatsu K, Hirose S, Yukitake K, Ogata H, Mitsudome A, Oda T. Relationship between maturation of the skin and electrical skin resistance. Pediatr Res. 1987;21:21–4.
67. Wojtaszek JL, Chatterjee N, Najeeb J, Ramos A, Lee M, Bian K, Xue JY, Fenton BA, Park H, Li D, et al. A small molecule targeting mutagenic translesion synthesis improves chemotherapy. Cell. 2019;178:152-159.e11.
68. Wong RP, García-Rodríguez N, Zilio N, Hanulová M, Ulrich HD. Processing of DNA polymerase-blocking lesions during genome replication is spatially and temporally segregated from replication forks. Mol Cell. 2020;77:3-16.e4.
69. van Bostelen I, van Schendel R, Romeijn R, Tijsterman M. Translesion synthesis polymerases are dispensable for C. Elegans reproduction but suppress genome scarring by polymerase theta-mediated end joining. PLoS Genet. 2020;16:1–20.
70. Nayak S, Calvo JA, Cong K, Peng M, Berthiaume E, Jackson J, Zaino AM, Vindigni A, Hadden MK, Cantor SB. Inhibition of the translesion synthesis polymerase REV1 exploits replication gaps as a cancer vulnerability. Sci Adv. 2020;6:eaaz7808.
71. Taglialatela A, Leuzzi G, Sannino V, Cuella-Martin R, Huang J-W, Wu-Baer F, Baer R, Costanzo V, Ciccia A. REV1-Polζ maintains the viability of homologous recombination-deficient cancer cells through mutagenic repair of PRIMPOL-dependent ssDNA gaps. Mol Cell. 2021;81:4008-4025.e7.
72. Tirman S, Quinet A, Wood M, Meroni A, Cybulla E, Jackson J, Pegoraro S, Simoneau A, Zou L, Vindigni A. Temporally distinct post-replicative repair mechanisms fill PRIMPOL-dependent ssDNA gaps in human cells. Mol Cell. 2021;81:4026-4040.e8.
73. Quinet A, Tirman S, Cybulla E, Meroni A, Vindigni A. To skip or not to skip: choosing repriming to tolerate DNA damage. Mol Cell. 2021;81:649–58.
74. Krijger PHL, van den Berk PCM, Wit N, Langerak P, Jansen JG, Reynaud C-A, de Wind N, Jacobs H. PCNA ubiquitination-independent activation of polymerase η during somatic hypermutation and DNA damage tolerance. DNA Repair. 2011;10:1051–9.
75. Hendel A, Krijger PHL, Diamant N, Goren Z, Langerak P, Kim J, Reißner T, Lee K, Geacintov NE, Carell T, et al. PCNA ubiquitination is important, but not essential for translesion DNA synthesis in mammalian cells. PLOS Genet. 2011;7: e1002262.
76. Murga M, Campaner S, Lopez-Contreras AJ, Toledo LI, Soria R, Montaña MF, D'Artista L, Schleker T, Guerra C, Garcia E, et al. Exploiting oncogene-induced replicative stress for the selective killing of Myc-driven tumors. Nat Struct Mol Biol. 2011;18:1331–5.
77. Koole W, Van Schendel R, Karambelas AE, Van Heteren JT, Okihara KL, Tijsterman M. A polymerase theta-dependent repair pathway suppresses extensive genomic instability at endogenous G4 DNA sites. Nat Commun. 2014;5:1–10.
78. Maya-Mendoza A, Moudry P, Merchut-Maya JM, Lee M, Strauss R, Bartek J. High speed of fork progression induces DNA replication stress and genomic instability. Nature. 2018;559:279–84.
79. Sharma S, Canman CE. REV1 and DNA polymerase zeta in DNA interstrand crosslink repair. Environ Mol Mutagen. 2012;53:725–40.
80. Deans AJ, West SC. DNA interstrand crosslink repair and cancer. Nat Rev Cancer. 2011;11:467–80.
81. Maddalo D, Manchado E, Concepcion CP, Bonetti C, Vidigal JA, Han Y-C, Ogrodowski P, Crippa A, Rekhtman N, de Stanchina E, et al. In vivo engineering of oncogenic chromosomal rearrangements with the CRISPR/Cas9 system. Nature. 2014;516:423–7.
82. Dirac AMG, Bernards R. Reversal of senescence in mouse fibroblasts through lentiviral suppression of p53. J Biol Chem. 2003;278:11731–4.
83. Ran FA, Hsu PD, Wright J, Agarwala V, Scott DA, Zhang F. Genome engineering using the CRISPR-Cas9 system. Nat Protoc. 2013;8:2281–308.
84. Chou T-C. Drug combination studies and their synergy quantification using the Chou-Talalay method. Cancer Res. 2010;70:440–6.
85. Li H, Durbin R. Fast and accurate short read alignment with Burrows-Wheeler transform. Bioinforma Oxf Engl. 2009;25:1754–60.
86. Cameron DL, Schröder J, Penington JS, Do H, Molania R, Dobrovic A, Speed TP, Papenfuss AT. GRIDSS: sensitive and specific genomic rearrangement detection using positional de Bruijn graph assembly. Genome Res. 2017;27:2050–60.
87. Auwera GAV. Genomics in the cloud Using docker, gatk, and wdl in terra. 2020.
88. Roepman P, de Bruijn E, van Lieshout S, Schoenmaker L, Boelens MC, Dubbink HJ, Geurts-Giele WRR, Groenendijk FH, Huibers MMH, Kranendonk MEG, et al. Clinical validation of whole genome sequencing for cancer diagnostics. J Mol Diagn JMD. 2021;23:816–33.
89. Review Commons Report 1. Early Evidence Base. 2024 https://doi.org/10.15252/rc.2024305769

90. Review Commons Report 2. Early Evidence Base. 2024. https://doi.org/10.15252/rc.2024611034
91. Review Commons Report 3. Early Evidence Base. 2024. https://doi.org/10.15252/rc.2024105892
92. Review Commons Response. Early Evidence Base. 2024. https://doi.org/10.15252/rc.2024202510
93. de Groot, D. (2024) Molecular dependencies and genomic consequences of a global DNA damage tolerance defect. Github; 2024 https://github.com/Daniel-Cornelis/Molecular-dependencies-and-genomic-consequences-of-a-global-DNA-damage-tolerance-defect.
94. de Groot, D. (2024) Molecular dependencies and genomic consequences of a global DNA damage tolerance defect. Zenodo; 2024 https://doi.org/10.5281/zenodo.14212067.
95. Netherlands Cancer Institute. Molecular dependencies and genomic consequences of a global DNA damage tolerance defect. https://www.ncbi.nlm.nih.gov/bioproject/PRJNA1017351
96. Hartwig Medical Foundation. https://www.hartwigmedicalfoundation.nl/en/data/data-access-request/

Publisher's Note